Proceedings of the Korean Nuclear Society Spring Meeting
Kwangju, Korea, May 2002

CHF Mechanism for Pool Boiling of R-113 on a Horizontal Heater

H. J. Chung [1], H. C. No[2], S. Y. Chun [1], and W. P. Baek [1]

[1] Korea Atomic Energy Research Institute
P.O. Box 105 Yusong, Daejon, 305-600, Korea

[2] Korea Advanced Institute of Science and Technology
373-1 Kusong-dong Yusong-gu, Daejon, 305-701, Korea

Abstract

A new experimental attempt was made to simultaneously observe the dynamic behavior of bubbles and dry spots in the vicinity of boiling surface. Also, the two-dimensional bubble structures were obtained separately. From the visualization results, the formation of bubbles and dry spots occur simultaneously. At CHF, the surface rewetting is repeated by the local nucleate boiling around the large vapor film. At just after CHF, nucleate boiling at the locally-wetted region is extinguished, resulting in the dryout of the whole heater surface. Therefore, we conclude that CHF is initiated from the locally-limited nucleate boiling activity rather than any hydrodynamic instability.

1. Introduction

In spite of extensive experimental and theoretical efforts there are still considerable disagreements regarding the boiling characteristics and critical heat flux (CHF) triggering mechanism. These disagreements come mainly from the lack of detailed knowledge of the physical phenomena causing the CHF on the near-wall region. As a result, almost all CHF models developed so far have described the CHF based on the postulated mechanisms, which were not verified through direct observation. Therefore, in order to describe the CHF triggering mechanism accurately, direct observation of the near-wall region during boiling crisis is very important.

As a classical visual study, Gaertner [1] directly observed the boiling phenomena in the near-wall region. He hypothesized the second transition region, where the stems of the vapor mushrooms collapse causing local vapor patches to form on the heat transfer surface. He concluded that widespread vapor patches caused CHF or burnout. Based on Gaertner's experimental observation, Haramura and Katto [2] proposed the 'macrolayer dryout model' and Dhir and Liaw [3] proposed the 'unified model' for CHF.

Dry spots or dry areas on the heating surface have been reported in a number of experimental results. The occurrence of dry areas means that the heating surface is partly in contact with the liquid. The

effect of dry areas on the heating surface is very important, because the dry areas have much poorer heat transfer rate than the surface covered with the liquid Nishio et al. [4] observed the dynamic behavior of dry area for the pool boiling of R-113 on a sapphire plate. They pointed out that the liquid–solid contact of the network pattern at CHF is much different from the observation of Gaertner [1], and the boiling structure model by Dhir and Liaw [3] and Haramura and Katto [2], in which isolated tiny vapor stems are attached to the boiling surface. Even though the dry spots were experimentally observed by a number of investigators as discussed above, they were not actively considered in CHF modeling so far. Very recently, Ha and No [5-7] successfully applied the behavior of dry spots to the development of CHF models.

It is evident from the above reviews that the bubble behaviors in each boiling subregime are closely related to the formation of dry areas, and these dry areas, at least, are responsible for the onset of CHF. Therefore, to obtain clear information for the CHF triggering mechanism, the synchronized observation for the behavior of bubbles and dry areas rather than the individual observation in the vicinity of a boiling surface is essential. In the present study new experimental attempts are made to directly observe the physical boiling phenomena of bubbles and dry areas simultaneously from the below the heater surface. In addition, we take side views of bubbles to obtain the two-dimensional bubble behavior.

2. Experimental Method

In the present study, two cases of direct observations for the boiling surface have been carried out. First, the synchronized dynamic behaviors of bubbles and dry areas (Experiment-1) were observed by using experimental facility-1. And experimental facility-2 was used to observe the lateral bubble structures (Experiment-2). In order to maintain the consistency between two experiments, all experimental conditions are kept the same.

2.1 Description of Experiment-1 for synchronized observation of dynamic behaviors of bubbles and dry areas

The experimental facility-1 was made for both pool and flow boiling tests. A schematic flow diagram of the experimental facility-1 is shown in Fig. 1. It consists of a test section, condenser, storage tank, canned motor pump, and preheater.

As shown in Fig. 2, the horizontal test section is made of 80x80 mm inner dimension mica plates that are 10 mm thick and 0.5 m long. A 10 mm thick and 50x50 mm square single crystal sapphire plate is installed on the central part of the bottom plate of the test section. The base surface of the sapphire plate is coated with a transparent electro-conductive (ITO: Indium Oxide with a trace of Tin Oxide) film of 700 angstroms. The bottom face of the heater, single crystal sapphire, is enclosed with the silicone oil bath to reduce the heat loss and to match the refractive index.

For the pool boiling test, two isolation valves at upstream and downstream of the test section are closed, and four auxiliary heaters, each of which has a maximum heat capacity of 450 W, maintains the liquid temperature as a saturation condition under atmospheric pressure.

A 250 volt, 8 ampere D.C. generator, supplies electric power to the electro-conductive film, then the test liquid is boiled on the upper surface of the sapphire plate. Six K-type thermocouples, four on the lower side and two on the upper side of the sapphire plate, measure both side heater surface temperatures.

An Ar-Ion laser is used as a light source. As shown in Fig. 2, the laser beam reflected from the mirror is introduced to the bottom of the sapphire plate. If this incident beam is adequately set, the total reflection will occur on the upper surface of the sapphire plate when the upper heated surface is dry, while it does not occur when the surface is wet by the liquid. At the same time, we directly observe the bubbles on the upper heater surface.

In this study R-113 was selected as a test liquid due to its low boiling point (47.6 ^{o}C at 0.1 MPa). The boiling experiment has been carried out under the steady state conduction by adjusting the DC current step by step. And the experimental ranges covered from low to high heat flux region (CHF). For each step, motion pictures were taken by a high-speed video system which was operated by 500 frames per second.

2.2 Description of Experiment-2 for observation of lateral bubble structures

To observe the bubble behavior from the lateral view, an experimental facility-2 is built up as illustrated in Fig. 3. As shown in Fig. 3(a), the test block is located in a rectangular glass vessel with inside dimensions of 150x150x200 mm. A test block, Fig. 3(b), is composed of a sapphire plate, a Teflon pad and a BK-7 glass plate. The boiling surface is basically the same as that of experiment-1. A 5mm thick and 40x5 mm single crystal sapphire plate, of which bottom face is coated with an ITO film of 700 angstroms thick, is settled down on a 3 mm thick teflon pad. The teflon pad together with a sapphire plate is put on a BK-7 plate with dimensions of 40x5x50 mm.

The visualization from the side of heater surface is stepwise repeated. The test liquid, conditions and method are the same as those of experiment-1. In this case, the temperature of the ITO film is obtained from its relationship between temperatures and resistances. And, the heater surface temperature is calculated from a steady-state conduction equation.

2.3 Confirmatory test

The primary objectives of the confirmatory test are first to examine the pertinence of the simultaneous visualization of bubbles and dry areas, second to evaluate the degree of distortion from image processing.

The bottom part of a glass sphere simulating a bubble was cut to represent a dry spot, and machined to settle down on the heater. The holes resulting from the cut down simulate the different size of dry spots. Diameters of the simulated bubbles and were measured carefully before experiments. The confirmation test was performed under non-heating condition by using the same method described in Section 2.1.

Figures 4 shows the simultaneous visualization results for the bubbles and dry spots. In this figure, the dry spots are clearly shown. Also, the bubbles viewed from direct observation have complete

spherical shapes, even though the optical path for direct reflection has some observation angle. From the image processing, it is noted that the diameters of the bubbles and dry spots have approximately 3 % and 4 % distortion, respectively, comparing to the real size of them. From the confirmatory test, we can conclude that the present optical method to simultaneously measure the bubble and dry spot sizes is very appropriate.

3. Experimental Results

3.1 Visualization results

3.1.1 Chronological behavior of bubbles and dry spots

Figure 5 shows the chronological sequence of bubbles and dry spots at the inception of boiling (ΔT_{ws}=21.4 K). Figures 5(a) and (b) show bubble nucleation and growth. Figures 5(c) and (d) are the situation at the moment before detaching, and finally the bubble disappears in the picture. The lower part of Fig. 5 shows the dynamic behavior of dry spots under the corresponding bubbles. When a bubble nucleates, a dry spot below it appears and exists while the bubble is growing. Finally, if the bubble is detached, the dry spot disappears instantaneously. From the present synchronized observation for the chronological behavior of bubbles and dry spots, it is noted that the dry spots and bubbles exist simultaneously. This means that when a bubble grows at a nucleation site, a dry spot is formed under the corresponding bubble.

3.1.2 Boiling regimes

Figures 6 and 7 show a typical set of observed boiling phenomena from incipience of boiling to CHF. The pictures in Fig. 6 are the results of the synchronized observation and in Fig. 7 are the side views of bubbles. The identification indices in Figs. 6 and 7 correspond to regimes in the boiling curve given in Fig. 8.

<u>Discrete bubble regime</u>

Figure 6(a) is a situation at incipience of boiling, and Figs. 6(b) and (c) shows the behavior of bubbles and dry spots at the discrete bubble region (ΔT_{ws}=23.9 K and 29.5 K, respectively). Comparing to the situation at incipience of boiling, many round-shaped discrete bubbles and dry spots are observed. At the early portion of the discrete bubble regimes, shown in Figs. 7(a) and (b), the interaction between bubbles does not distort the shape of them. Figure 7(c) shows that their interaction at some higher heat fluxes retards the departure of bubbles and their shape is slightly distorted, but a discrete bubble regime is maintained. In this discrete bubble regime, the distinct feature is that the active site density is exactly the same as the dry spot density. The discrete bubble regime continues up to approximately 70% of CHF.

Coalesced bubble regime

At heat fluxes above 70% of CHF, the interaction between bubbles occurs actively. Figure 6(d) represents the situation at approximately heat fluxes of 80% of CHF (ΔT_{ws}=34.1 K, q=112.1 kW/m^2). Due to the lateral interaction between bubbles, some coalesced dry areas are observed to be larger than that of an isolated dry spot. The interaction process is clearly seen in Fig. 7(d). Even though some large dry areas are observed on the heater surface, the slope of boiling curves does not change apparently as shown in Fig. 8. From the video image analysis, the time-averaged resident time of large dry areas for the coalesced bubble regime is within 4 ms for the present study. Therefore, it is considered that the surface temperature does not increase during the short period of the large dry area.

Local vapor film regime (ΔT_{ws}=34.1 K and q=112.1 kW/m^2)

As the heat flux is increased above 80% of CHF, the bubble behaviors are somewhat different from those of the preceding heat flux cases as shown in Figs. 6(e) and 7(e). Most bubbles are coalesced each other, and their shape seem like vapor patches. As a result, the intensive interaction between dry areas occurs. Bubble behaviors observed from side window are illustrated sequentially in Fig. 9. Under a large departing vapor mass, a filmwise vapor bubble formed from the lateral coalescence of bubbles exists locally. The occurrence of the local filmwise vapor bubble results in the formation of the even larger dry area. And, the resident time of the large dry area under the filmwise vapor bubble is further increased comparing to those of the preceding heat flux regimes. This increased resident time of the large dry area influences the heat transfer mechanism and, consequently, the slope of the boiling curve becomes mild as marked (e) in Fig. 8.

Critical heat flux (ΔT_{ws}=43.0 K, q=139.9 kW/m^2)

In the present study, the CHF was defined as the highest heat flux that the heater surface temperature was kept stable before temperature excursion was commenced by a slight increase in heat flux. Figure 10 shows the chronological dynamic behavior of bubbles and dry areas at CHF. As shown in Fig. 10, most of the heater surface becomes dry and the liquid-solid contact fraction decreases below 30% as shown in Fig. 13. In this situation the dry areas behave very violently with enlarging and shrinking. As a result, considerable interaction between dry areas occurs. During the violent behavior of dry areas, the wetted pattern is not a continuous plane type but maze-like curves. This wetted pattern is similar to the network pattern observed Nishio et al. [4]. At the same time, the vigorous boiling occurs in wetted regions.

The side views of bubble structures at CHF are shown in Fig. 11. A large vapor film covers a great part of heater surface. However, intense nucleate boiling takes place around the edge of the vapor film. Some nucleating bubbles in a locally-wetted region coalesce laterally each other and form another small vapor film. This small vapor film does not grow large, and a wetting region is formed repeatedly. This type of local nucleate boiling is similar to the observation by Galloway and Mudawar [8] for flow boiling of FC-72.

A large vapor film, which covers a great part of the heater surface, collapses when its upper interface departs. After the large vapor film collapses, a short wetting occurs as shown in Fig. 11(c). If the surface is intermittently wetted, vigorous boiling occurs and a continuous vapor film resulting from the coalescence of vapor bubbles is reestablished as shown in Fig. 9(e). This phenomenon is similar to the observation by Nishio et al. [4]. From the above photographic analysis, it is noted that, even though the vapor film covers a large fraction of the heater surface, the local nucleate boiling in the wetted region plays a key role in determining the heater surface temperature not increasing further.

CHF triggering mechanism

At CHF, the slight increase of heat flux causes a commencement of temperature excursion. This situation just after CHF is called as CHF(+). Photographs for CHF(+) are shown in Fig. 12. Even though the wavy motion of the large vapor film occurs actively, the liquid does not touch the heater surface, resulting in no wetting. Also, the formation of the wetted region due to the departure of a large vapor film, which is repeatedly seen at CHF, is not observed as in the case of CHF(+), while brief nucleate boiling occurs at the edge of a vapor film as illustrated in Figs. 12(a), (b) and (c). However, the wetted region quickly becomes the dry region with a continuous vapor film and then nucleate boiling is limited as shown in Fig. 12(d).

From comparing the side views of bubble behaviors, some distinct differences in wetting modes between CHF and CHF(+) can be drawn. As described, at CHF, liquids were intermittently supplied to the surface through the repeated formation and collapse of the relatively small vapor film at the edge of the large one. Unlike CHF situation, there is little liquid penetration during the departure of a large vapor mass at CHF(+). Brief nucleate boiling is observed only at the wetted region near the edge of the vapor film as shown in Figs. 12(a), (b) and (c). However, this brief wetting is extinguished by an agglomeration of nucleating bubbles as in Fig. 12(d). As a result of this limited nucleating boiling activity at the local wetted part of the heater surface, the heater surface temperature begins to increase further. Consequently, even though the surface temperature is well below the Leidenfrost temperature, the rewetting is precluded due to the agglomeration of nucleating bubbles at the local wetted region. These observations are similar to the localized reduced boiling activity by Galloway and Mudawar [8] and Celata et al. [9]. Once the continuous vapor film covers the whole heater surface, no nucleate boiling appears on the heater surface and the surface temperature begin to rise slowly from a stable value of approximately 90 ^{o}C. However, once the surface temperature exceeded approximately 108 ^{o}C, it begins to rise uncontrollably at a very faster rate. Finally burnout occurred. As discussed above, CHF(+) comes from the locally-limited nucleate boiling activity rather than any changes of hydrodynamic conditions. This physical phenomenon is contrary to the vapor jet model proposed by Zuber [10] and Lienhard and Dhir [11].

3.2. Wall temperature measurement

Figure 14 shows the time- and space-averaged surface temperature as a function of the heat flux along with the corresponding boiling subregime boundaries. In the early portion of the nucleate

boiling region, the wall temperature curve is almost linear. As soon as the number of nucleating bubbles increases, the slope of the wall temperature curve apparently reduces and becomes flat. However, in the local vapor film regime, the slope of the temperature curve increases abruptly. This implies that the large dry area under the large vapor bubble contributes to the increase of the surface temperature. As heat flux is increased further, the stable filmwise bubbles cover the whole heater surface. Consequently, the nucleation of bubbles is limited and the surface temperature increases uncontrollably.

3.3 Active nucleation site density

In this study, the active site density is counted only within the heat fluxes 80% of CHF. Above 80% of CHF, the counting of dry areas is impossible due to the intensive interaction. Figure 15 shows the time-averaged active site density during 200 ms as a function of the surface superheat. The active site density increases drastically with the increase of wall superheat. However, the trend is nearly linear. The active site density is the order of 10^5 in the fully-developed nucleate boiling region, and this result is nearly the same as that of case of 18 degrees by Wang and Dhir [12].

4. Conclusions

In the present study new experimental attempts are made to directly observe the physical boiling phenomena of bubbles and dry areas simultaneously from the bottom of the heater surface. In addition, we take the side views of bubbles to obtain the two-dimensional bubble behavior. From synchronized high-speed video imaging of bubbles and dry spots and the side views of bubble behaviors, the following conclusions can be derived:

1) The formation of bubbles and dry spots occur simultaneously. This indicates that when a bubble nucleates and grows at a nucleation site, a dry spot is formed under the corresponding bubble. Therefore, they should be considered as a synchronized identity rather than an independent one.
2) The dry spot density is equal to the active site density up to region 70% of CHF heat flux.
3) At CHF, the fraction of the dried area of the heater surface is above 70%. Also, the heater surface temperature is stably maintained due to the local nucleate boiling in the strip-shape wetted region existing around the edge of the vapor film, which has a capability to sufficiently extract the heat generated in the heater. As a result, we can conclude that CHF is strongly related to the locally-limited nucleate boiling activity at the wetted region rather than any hydrodynamic instability
4) At CHF(+), the nucleate boiling region still exists but the rewetting region is extinguished by an agglomeration of nucleating bubbles. Then, dry spots under the agglomerated bubble grows, eventually resulting in the dryout of all heater surface. At CHF(+), as the heat rate extracted from the wall by nucleate boiling becomes smaller than the energy production rate in the heaters, the heater surface temperature begins to increase.

Acknowledgement

This work was financially supported by the nuclear R&D program from the Ministry of Science and Technology of Korea.

References

[1] R. F. Gaertner, Photographic study of nucleate boiling on a horizontal surface, ASME Journal of Heat Transfer 87 (1965) 17-29.

[2] Y. Haramura, Y. Katto, A new hydrodynamic model of critical heat flux, applicable widely to both pool and forced convection boiling on submerged bodies in saturated liquids, International Journal of Heat and Mass Transfer 26 (1983) 389-399.

[3] V. K. Dhir, S. P. Liaw, Framework for a unified model for nucleate and transition pool boiling, ASME Journal of Heat Transfer 111 (1989) 739-746.

[4] S. Nishio, T. Gotoh and N. Nagai, Observation of boiling structures in high heat-flux boiling, International Journal of Heat and Mass Transfer 41 (1998) 3191-3201.

[5] S. J. Ha, H. C. No, A dry-spot model of critical heat flux in pool and forced convection boiling, International Journal of Heat and Mass Transfer 41 (2) (1998) 303-311

[6] S. J. Ha, H. C. No, A dry-spot model for transition boiling heat transfer in pool boiling, International Journal of Heat and Mass Transfer 41 (1988) 3771-3779.

[7] S. J. Ha, H. C. No, A dry-spot model of critical heat flux applicable to both pool boiling and subcooled forced convection boiling, International Journal of Heat and Mass Transfer 43 (2000) 241-250.

[8] J. E. Galloway, I. Mudawar, CHF mechanism in flow boiling from a short heated wall-I. Examination of near-wall conditions with the aid of photomicrography and high-speed video imaging, International Journal of Heat and Mass Transfer 30 (10) (1993) 2511-2526.

[9] G. P. Celata et al., Visual investigation of high heat flux burnout in subcooled flow boiling of water, Third International Conference on Multiphase Flow, ICMF'98, Lyon, France, 1998.

[10] N. Zuber, Stability of boiling heat transfer, ASME Journal of Heat Transfer 80 (1958) 711-720.

[11] J. H. Lienhard and V. K. Dhir, Hydrodynamic predictions of peak pool-boiling heat fluxes from finite bodies, ASME Journal of heat Transfer 95 (1973) 152-158.

[12] C. H. Wang and V. K. Dhir, Effect of surface wettability on active nucleation site density during pool boiling of water on a vertical surface, ASME Journal of Heat Transfer 115 (1993) 659-669.

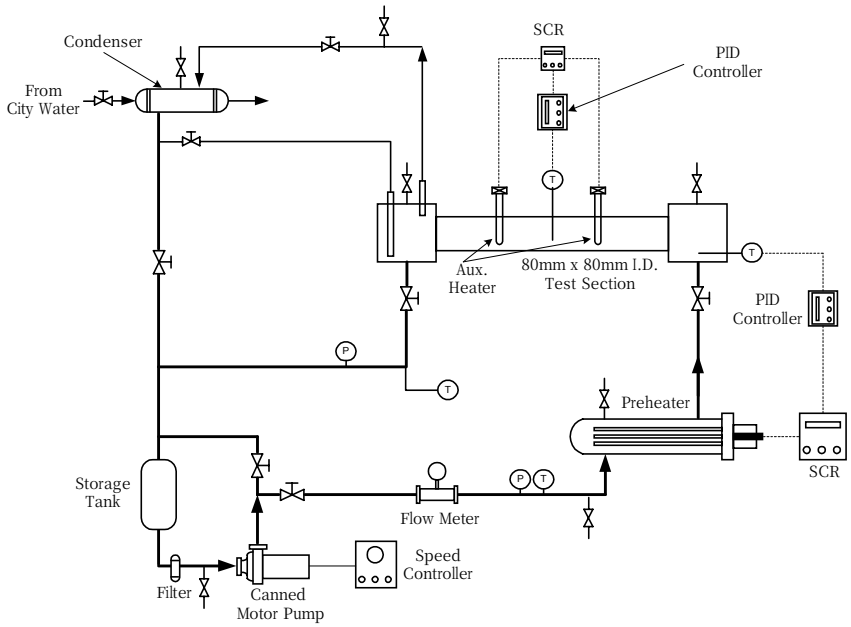

Fig. 1. Schematic flow diagram of the boiling test facility.

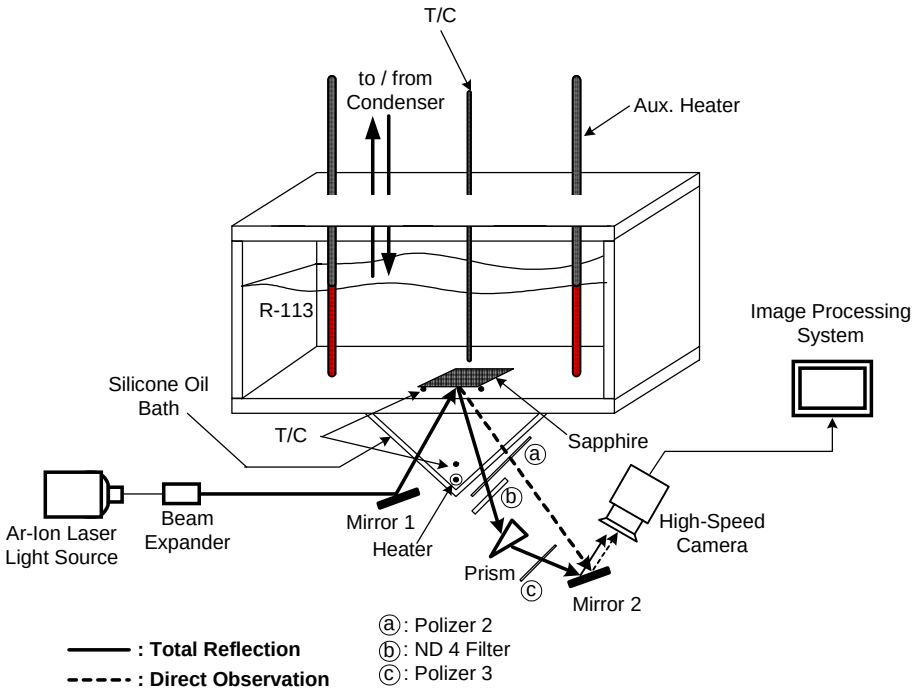

Fig. 2. Configuration of the test section with optical setup for pool boiling test.

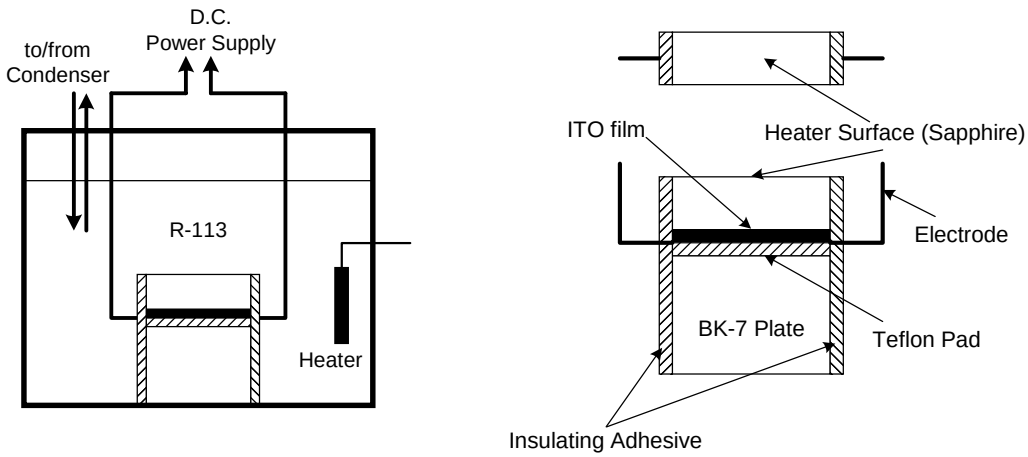

(a) Experimental apparatus (b) Boiling surface

Fig. 3. Schematic diagram of the test apparatus to observe the side views of bubble structures.

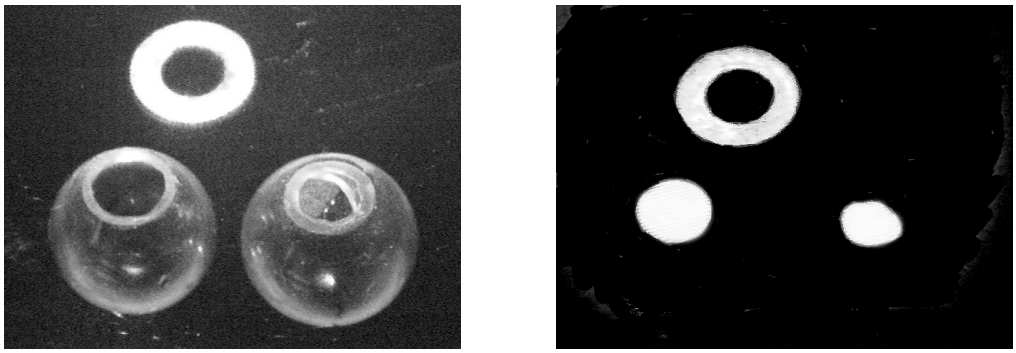

(a) Bubble (b) Dry Spot

Fig. 4. Confirmatory test results: simultaneous visualization of bubbles and dry spots

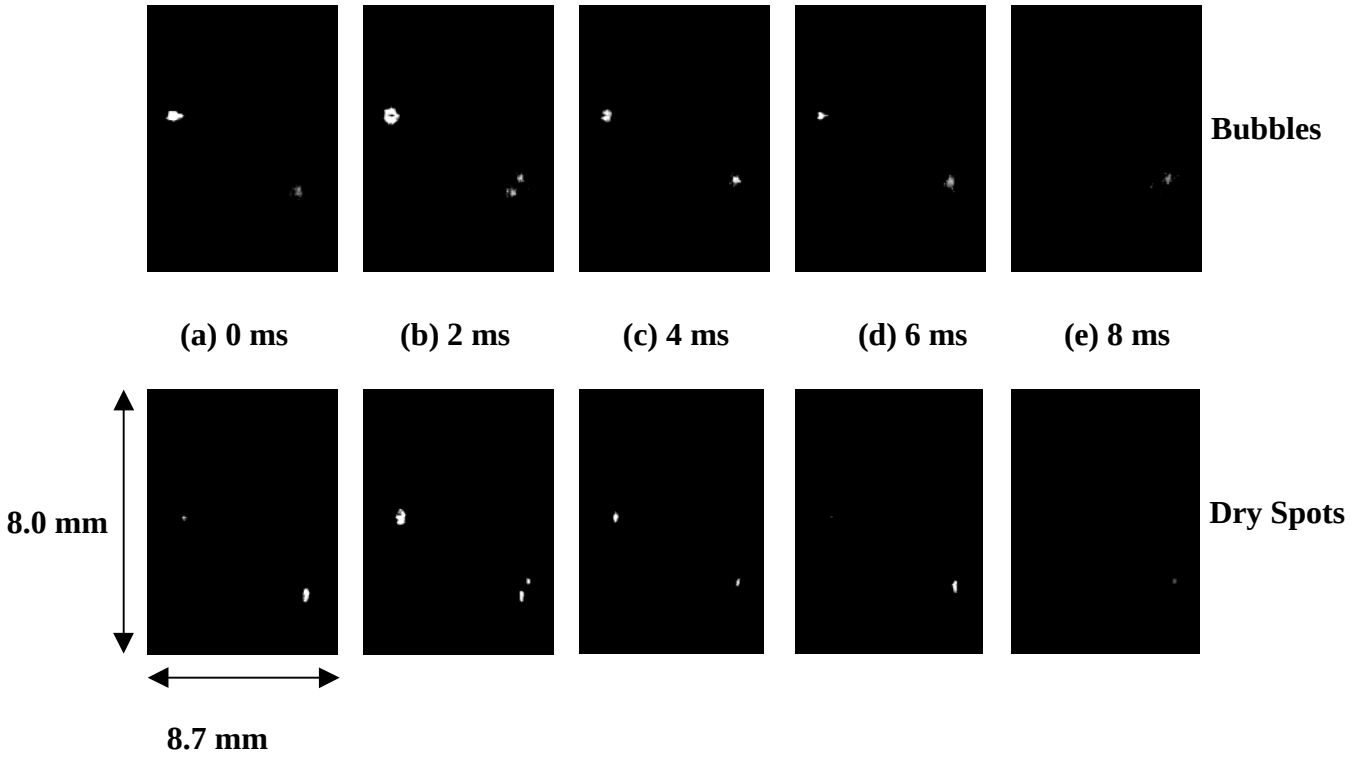

Fig. 5. Chronological dynamic behavior of bubbles and dry spots at incipience of boiling.

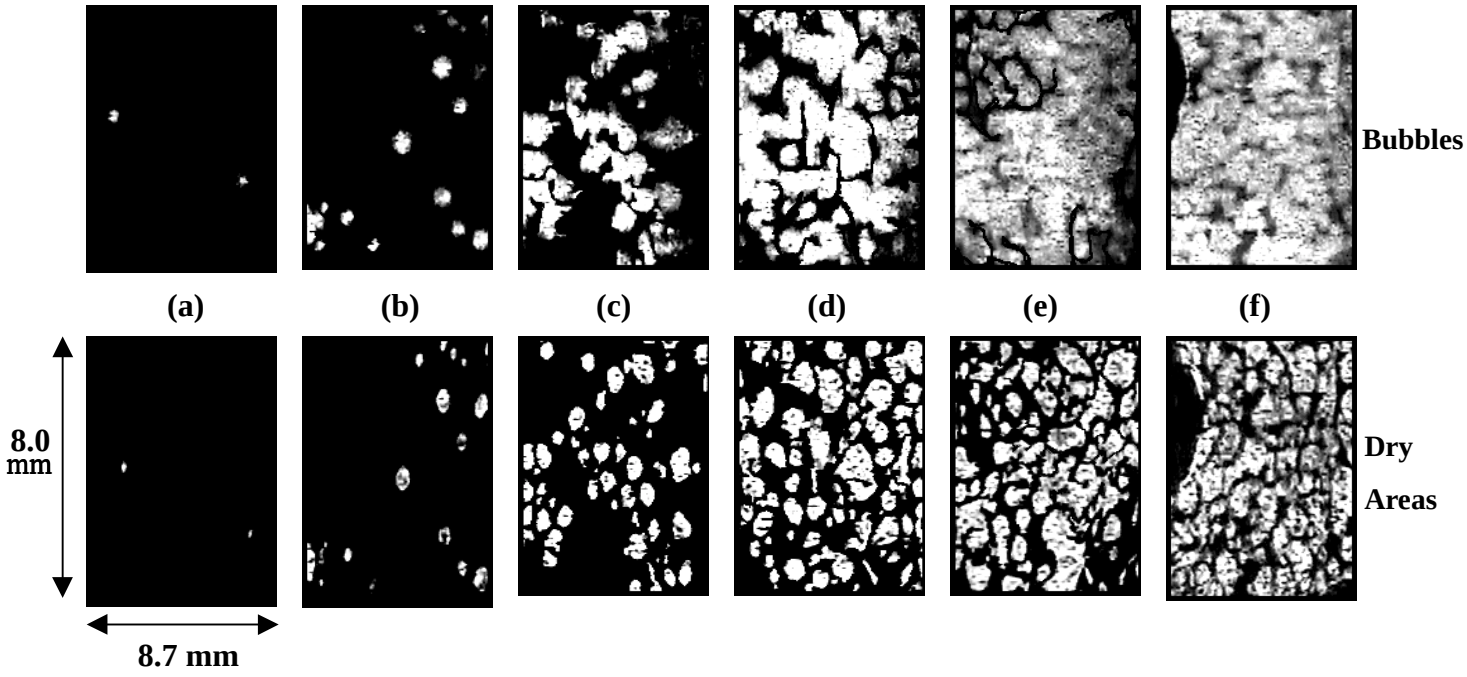

Fig. 6. Variations of bubbles and dry areas from incipience of boiling to CHF.

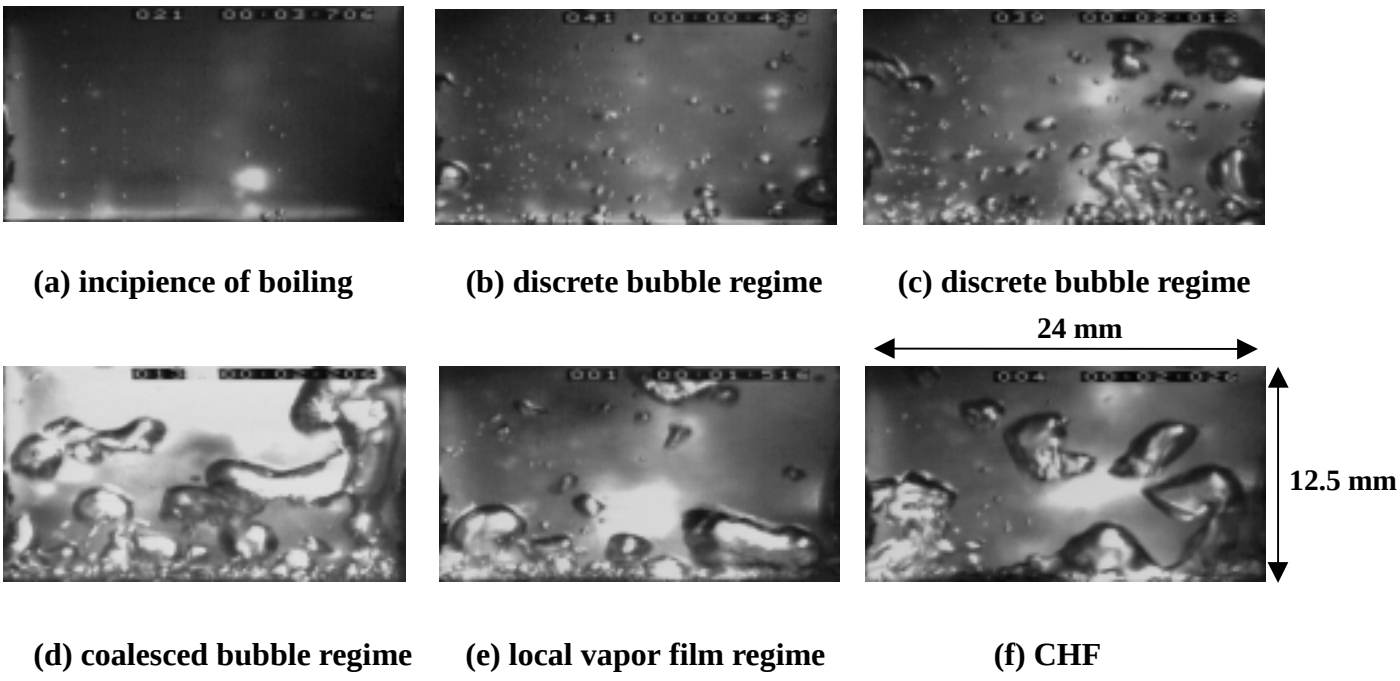

Fig. 7. Side views of bubble structures at each step of heat flux.

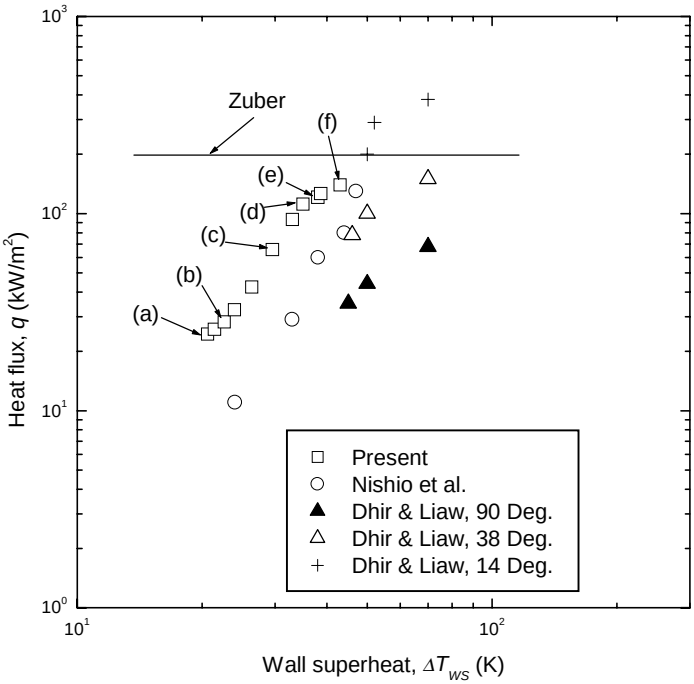

Fig. 8. Boiling curve for the present study with another predicted and measured ones.

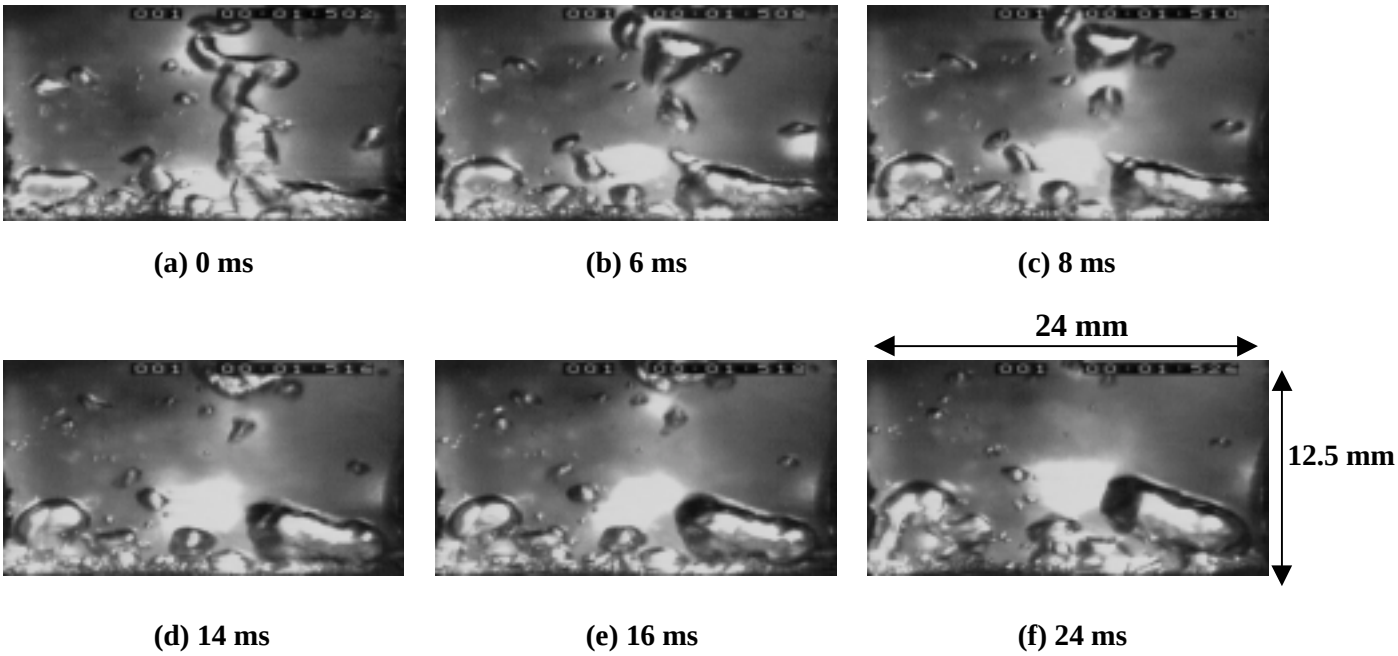

Fig. 9. Side views of dynamic behavior of bubbles at local vapor film regime (q = 0.9 q_{CHF}).

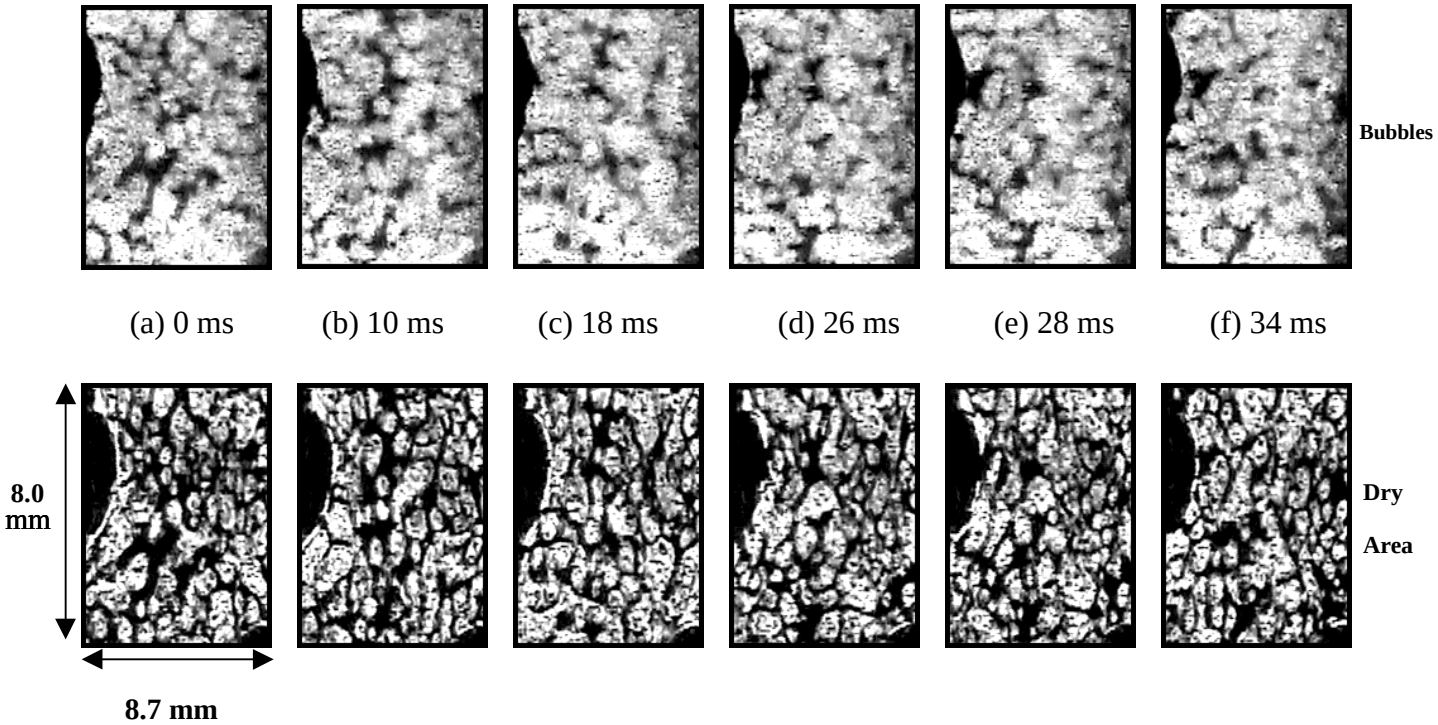

Fig. 10. Chronological dynamic behavior of bubbles and dry areas at CHF.

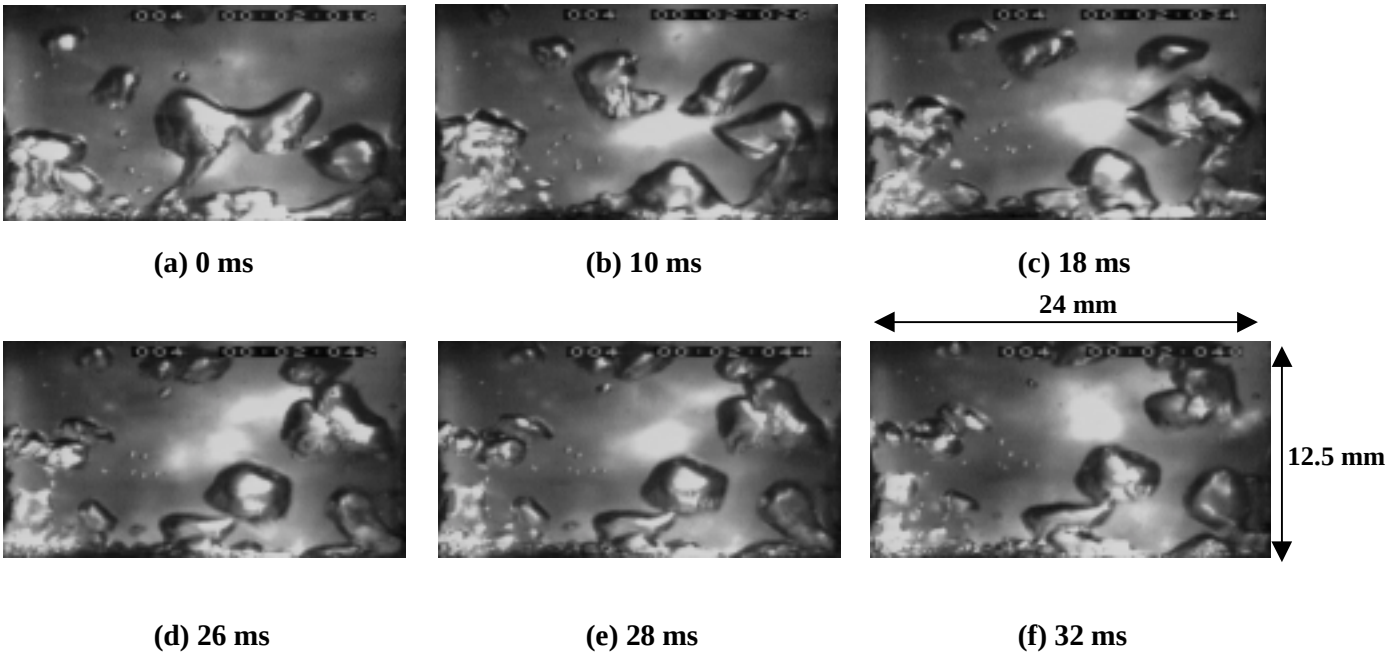

Fig. 11. Side views of dynamic behavior of bubbles at CHF.

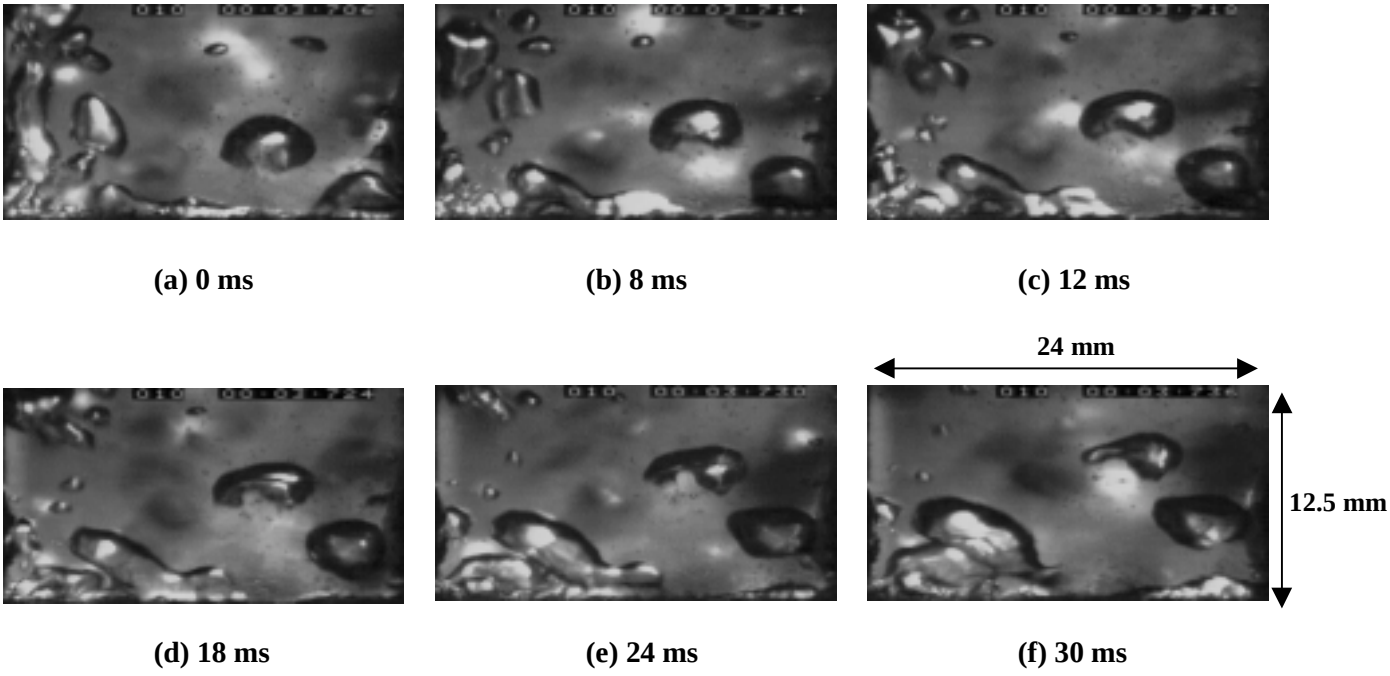

Fig. 12. Side views of dynamic behavior of bubbles just after CHF (q = 1.06q_{CHF}).

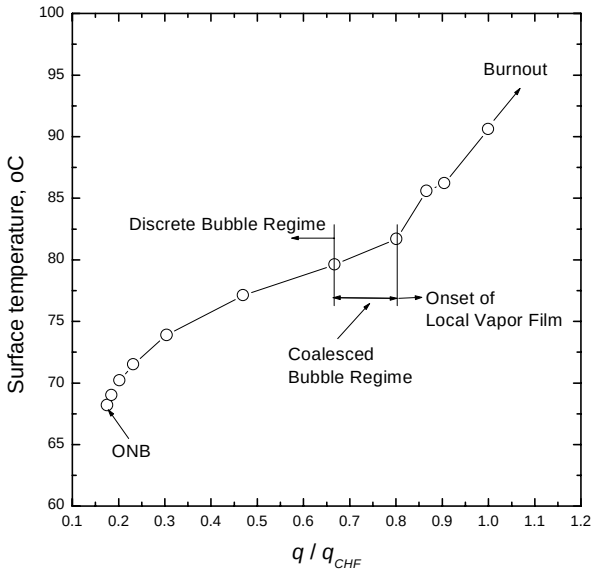

Fig. 13. Wetted fraction as a function of the surface superheat.

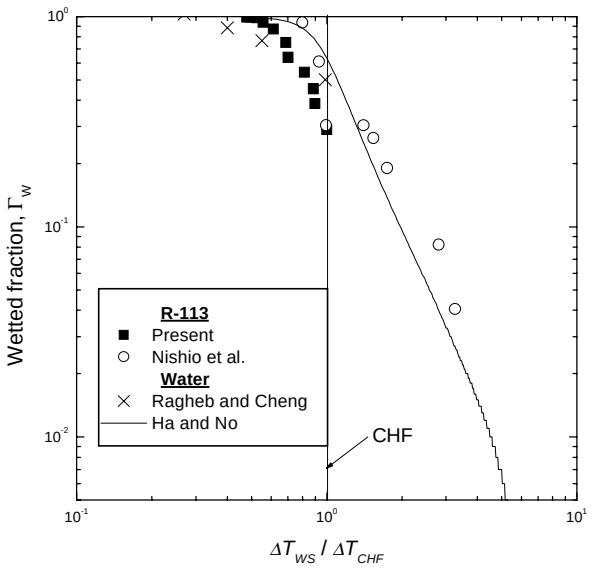

Fig. 14. Measured heater surface temperature as a function of the heat flux.

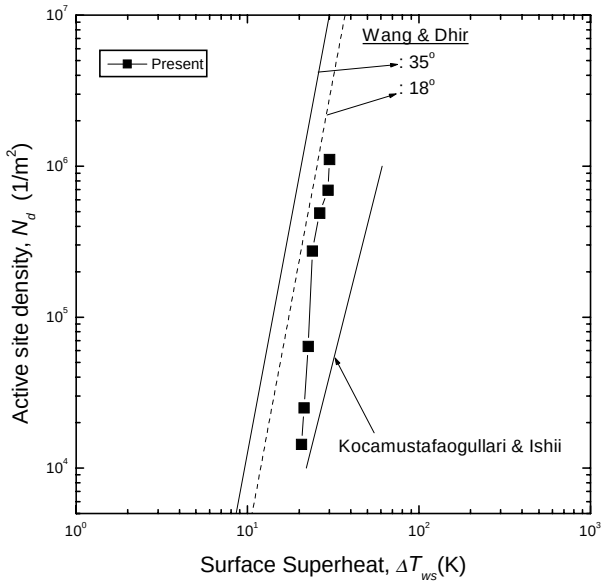

Fig. 15. Active site density as a function of the surface superheat.